Breakup Dynamics for High-Viscosity Droplet Formation in a Flow-Focusing Device: Symmetrical and Asymmetrical Ruptures

Wei Du, Taotao Fu, Chunying Zhu, and Youguang Ma
State Key Laboratory of Chemical Engineering, Collaborative Innovation Center of Chemical Science and Engineering (Tianjin), School of Chemical Engineering and Technology, Tianjin University, Tianjin 300072, China

Huai Z. Li
Laboratory of Reactions and Process Engineering, University of Lorraine, CNRS, 1, rue Grandville, BP 20451, 54001 Nancy Cedex, France

DOI 10.1002/aic.15043
Published online September 25, 2015 in Wiley Online Library (wileyonlinelibrary.com)

The breakup mechanism of high-viscosity thread for droplet formation in a flow-focusing device is investigated using a high-speed digital camera. Aqueous solution of 89.5%-glycerol is used as the dispersed phase, while silicone oil as the continuous phase. The breakup process of the dispersed thread presents two categories: symmetrical rupture and asymmetrical rupture. Furthermore, the rupture behavior could be divided into two stages: the squeezing stage controlled by the squeezing pressure and the pinch-off stage controlled by viscous stresses of both phases and surface tension. Specifically, it suggests that the differences in the shape of the liquid–liquid interface and the dynamics in the two breakup processes are caused by the disparity of the strain field at the point of detachment. Moreover, the thinning rate and the dynamics of the dispersed thread change with the viscosity of the continuous phase, but are less dependent of the flow rate of the continuous phase. © 2015 American Institute of Chemical Engineers *AIChE J*, 62: 325–337, 2016
Keywords: high-viscosity droplet, breakup, microfluidics, interface, confinement

Introduction

In recent years, microfluidic technology has attracted widespread attention and now it has been used in various applications such as emulsification, drug encapsulation, materials synthesis, crystallization, and chemical reactions owing to the characteristics of safety, high efficiency, and ease to control.[1–3] In the applications mentioned above, the high-viscosity droplets are frequently encountered and the monodispersity of the droplets usually determines the quality of the product. For example, the droplets' monodispersity has significant influence on the release of pharmaceuticals, emulsions ageing, and the refreshing feeling of a cosmetic lotion, and so forth.[4–6] As the rupture behavior affects the size and the polydispersity of the droplets,[5,7,8] it is of great significance to study the breakup mechanism of high-viscosity thread for droplet formation in microfluidic devices.

The breakup mechanism of dispersed thread for droplet formation under macroscopic scale has been systematically studied by investigating the dynamical behaviors of the dispersed thread (Table 1).[7,9–11,16–24] The dynamics and profile shape of the thread of the dispersed phase depend closely on the viscosity of fluids. When the effect of viscosity of the external fluid is negligible, there are three types of rupture behaviors: (1) If the viscosity could be ignored for the thread of the dispersed phase, the dynamics is in the "potential flow" regime. In this case, based on the asymptotic balance between the surface tension and inertia in the dispersed thread,[7,9] the variation of the minimum width w_m of the dispersed thread with the remaining time $(T-t)$ could be described by a power-law relation: $w_m \propto (T-t)^{2/3}$, where T is the formation period of the droplet and t represents the time. Moreover, the profile shape is asymmetrical. (2) If the thread of the dispersed phase has a high viscosity, the variation of the minimum width of the dispersed thread with the remaining time near-pinching could be scaled as a linear relationship: $w_m = k\frac{\sigma}{\mu_d}(T-t)$, where k is a proportionality factor, σ the interfacial tension and μ_d the viscosity of the dispersed phase. In this situation, if the inertia in the thread could be ignored, the dynamics might fall in the "viscous thread" regime, and the shape of the dispersed thread is cylindrical with $k = 0.0709$.[21] (3) The dynamics would be in the "inertial-viscous" regime when the inertial effect of the high-viscosity dispersed thread cannot be ignored. The shape of the interface is asymmetrical, and the value $k=0.0304$ predicted by an asymptotic balance between inertial, viscous, and capillary forces.[22] Additionally, if the influence of the viscosity of the external fluid cannot be ignored, the "Stokes flow" regime will occur, and the viscous stress must be considered no matter how small the external fluid viscosity is. In this

Correspondence concerning this article should be addressed to T. Fu at ttfu@tju.edu.cn or Y. Ma at ygma@tju.edu.cn.

© 2015 American Institute of Chemical Engineers

Table 1. Experimental Studies on the Dynamics of the Thread of the Dispersed Phase in Macroscale and Microscale

Macroscale

Authors	Viscosity μ_c (mPa·s)	Viscosity μ_d (mPa·s)	μ_d/μ_c	Correlation	Forces	Droplet/Bubble	Dynamic Regime
Chen et al.[9]	0.018	1	55	$w_m \propto (T-t)^{2/3}$	surface tension ~ inertia	Droplet	"potential flow" regime
Rothert et al.[10]	0.018	99	5500	$w_m = 0.709 \frac{\sigma}{\mu_d}(T-t)$	viscous stress of the dispersed phase ~ surface tension	Droplet	"viscous thread" regime
Chen et al.[9] Rothert et al.[10]	0.018	85, 99	4722, 5500	$w_m = 0.304 \frac{\sigma}{\mu_d}(T-t)$	Inertial ~ viscous ~ capillary forces	Droplet	"inertial-viscous" regime
Cohen et al.[11]	1000	950	0.95	$w_m = k(\lambda) \frac{\sigma}{\mu_d}(T-t)$	viscous stresses of both phases ~ surface tension	Droplet	"Stokes flow" regime

Microscale

Authors	Viscosity μ_c (mPa s)	Viscosity μ_d (mPa s)	μ_d/μ_c	Correlation	Forces	Droplet/Bubble	Microfluidic Device
Garstecki et al.[8]	1–10	0.018	0.0018–0.018	$w_m \propto t$	Squeezing pressure	Droplet/bubble	Flow-focusing devices with a small orifice
Dollet et al.[12]	1	0.018	0.018	$w_m \propto (T-t)^{1/3}$	Inertia of both phases	Bubble	Flow-focusing devices with a small orifice
Fu et al.[13]	0.92, 2.32, 10.18	11, 103	1–12	$w_m \propto (T-t)^{\alpha}$ $\alpha = 0.32$–0.34 for low Re $\alpha = 0.52$–0.73 for high Re	——	Droplet	Flow-focusing devices
Fu et al.[13]	0.92	103	112	$w_m \propto T$	——	Droplet	Flow-focusing devices
Arratia et al.[14]	240	$\mu_N = \mu_{NN} = 240$	1	$w_m \propto \exp(t)$	Stress balance between inside and outside the interface	Droplet	Flow-focusing devices
Arratia et al.[14]	240	$\mu_N = \mu_{NN} = 240$	1	$w_m \propto t$	Radial stress ~ Laplace pressure	Droplet	Flow-focusing devices
Steinhaus et al.[15]	10	$\mu_N = \mu_{NN} = 6$	0.6	$w_m \propto (T-t)^{2/3}$	Surface tension ~ inertia	Droplet	Flow-focusing devices with a small orifice
Steinhaus et al.[15]	10	$\mu_N = \mu_{NN} = 6$	0.6	$w_m \propto \exp(t)$	Elastocapillary balance	Droplet	Flow-focusing devices with a small orifice
This work	50, 100, 200	153.7	0.77–3.07	$w_m \propto (T-t)^{\alpha}$ $\alpha = 0.29$–0.67	——	Droplet	Flow-focusing devices
This work	50, 100, 200	153.7	0.77–3.07	$w_m \propto (T-t)^{0.669}$	viscous stresses of both phases ~ surface tension	Droplet	Flow-focusing devices
This work	50, 100, 200	153.7	0.77–3.07	$w_m \propto t$	viscous stresses of both phases ~ surface tension	Droplet	Flow-focusing devices

Remarks: N represents Newtonian liquid; NN represents viscoelastic liquids.

regime, the shape of the pinching region is conical. And based on the asymptotic balance between the surface tension and viscous stresses of the two fluids,[7,11,24] the minimum width of the thread of the dispersed phase decreases linearly with the remaining time as $w_m = k(\lambda)\frac{\sigma}{\mu_d}(T-t)$, where $k(\lambda)$ is a dimensionless function depending on the viscosity ratio λ for the dispersed phase to the continuous phase. As reported previously, the dynamics of the breakup process may shift from one regime to another as the width of the dispersed thread evolves during the droplet formation.[9,23]

In comparison to the macroscopic scale, both the external fluid flow and the confinement of the channel, as well as the viscosity of fluids, have significant effects on the droplet generation in the microscopic scale. When the capillary number of the continuous phase $Ca_c < 10^{-2}$, the drop formation is controlled by the squeezing mechanism,[8,25] where the shear stress of the continuous phase has almost no influence on the breakup process and the droplet formation is driven by the pressure of the continuous phase. The droplet size depends only on the flow rates of two phases.[25] When $Ca_c > 10^{-2}$, the shearing mechanism is predominant, where the shear force of the continuous phase plays an important role, and the droplet formation is dominated by the balance between the viscous shear force and surface tension.[24] In addition, a transient regime was proposed recently, where the droplet formation is controlled by a combination of squeezing mechanism and shearing mechanism.[26,27]

To gain insight into the droplet formation in microscale, the dynamical behaviors of the thread of the dispersed phase have also been investigated in microfluidic devices as shown in Table 1. It is known that both the cross-sectional shape of the microchnnel and the initial conditions, such as the flow rate and the viscosity of liquids, could influence the breakup dynamics of the neck of the dispersed phase. In a flat microchannel with w_c/h=1-5, where w_c and h are the width and depth of the channel respectively, the breakup of the low-viscosity dispersed thread surrounded by low-viscosity liquids goes through a slow linear two-dimensional (2-D) collapse ($w_m \propto t$) when the interface is confined by the channel, and then ends in a fast three-dimensional (3-D) nonlinear pinch-off ($w_m \propto (T-t)^{1/3}$) when the interface detaches from the wall.[8] Nevertheless, the low viscosity dispersed thread only undergoes a 3-D pinch-off ($w_m \propto (T-t)^{1/3}$) in the microchannel with a square cross-section.[12] It is also worth noting that the process of 3-D collapse with the exponent 1/3 is driven by the inertia of both phases.[12] However, the exponent is 1/2 when the variation of the neck width is unaffected by the dynamical radial pressure imposed by the flow of the continuous phase.[18] In addition, Fu et al.[13] indicated that the exponent is related to the initial conditions for the low-viscosity droplets formation in square microchannels, and the dispersed thread decreases linearly with time $w_m \propto t$ when the viscosity of the dispersed phase is high. Nevertheless, for the high-viscosity droplet formed in another high-viscosity fluid, the scaling law and the driving forces for the evolution of the dispersed thread are distinct in the two dynamic regimes.[14]

Although several efforts have been devoted to studying the breakup mechanism of the dispersed thread for droplet formation in microscale, the effects of the viscosities of both phases on the dynamics of droplet formation, especially the high-viscosity droplet, in the microchannel have not yet been fully understood. In addition, the study on the dynamical behaviors associated with the high viscosity droplet formation would allow a better understanding of the driving mechanism for the droplet formation in complex fluids,[14,15] such as viscoelastic fluid, shear thinning fluids or yield stress fluids. This can facilitate its potential applications in drug delivery, crystallization, materials synthesis, and so forth.[15]

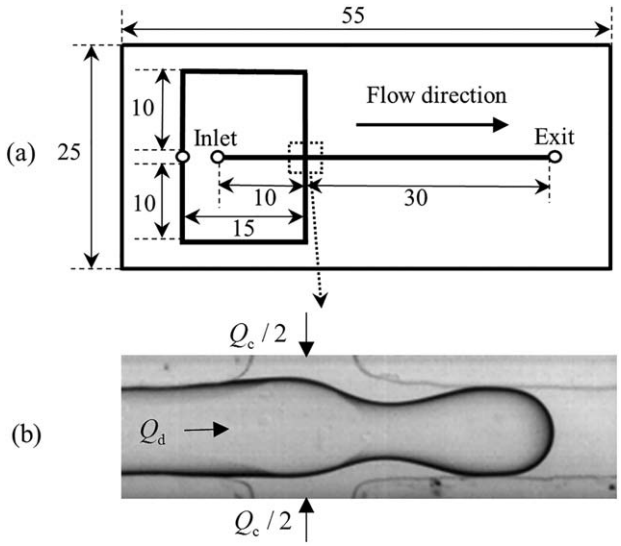

Figure 1. (a) Schematic diagram of the microfluidic device. All the cross-sections of these microchannels are 200 μm (height) × 200 μm (width). Unit: mm. (b) Water droplets are generated at the intersection of microfluidic device (dashed line box in Figure 1a).

In this work, the breakup process of the dispersed thread for high-viscosity aqueous phase droplets formed in high-viscosity silicone oils in a flow-focusing device is studied. Furthermore, the effects of the flow rate and viscosity of the continuous phase on the thinning rate and the dynamical behaviors of the thread of the dispersed phase are also investigated. Compared to the previous work with high-viscosity liquids,[5,28] this study is mainly focused on the breakup dynamics of the high-viscosity dispersed thread instead of the flow pattern or the size of the formed droplets. The study on the interfacial dynamics is an effective and intuitive method to understand the mechanism for droplet formation. Furthermore, this work also emphasizes the importance of the fluid flow and the viscosity of the continuous phase to the breakup dynamics and the profile shape of the liquid–liquid interface, which is always neglected in the study under macroscopic scale. This study could serve as a complement for previous work on the breakup mechanism during the process of the high-viscosity droplet formation in microchannel.

Experimental Procedure

The microfluidic device used in this work is shown in Figure 1. The microchannel with the square cross-section of 200 μm × 200 μm enables the dispersed thread to undergo a 3-D collapse during the droplet formation.[12,29,30] The device was fabricated by a soft lithography technique using polydimethylsiloxane (PDMS) as the channel material. The PDMS surface was treated with plasma technology and then bonded to a glass cover plate. Three holes (d=1mm) were drilled into the PDMS surface, and stainless steel tubes (d_i=1mm) were used to connect the inlets and outlet of the microchannel to tygon tubes (ID = 1.02 mm). The dispersed phase was introduced from the main channel at a flow rate of Q_d and the continuous

Table 2. Physical Properties of Various Liquid–Liquid Systems Used

Pair	Disperse Phase	Density ρ_d (kg m^{-3})	Viscosity μ_d (mPa s)	Continuous Phase	Density ρ_c (kg m^{-3})	Viscosity μ_c (mPa s)	Interfacial Tension σ (mN m^{-1})	λ
1	89.5% glycerol	1229	153.7	Silicone oil	957.2	50	34.2	3.07
2	89.5% glycerol	1229	153.7	Silicone oil	961.4	100	37.1	1.54
3	89.5% glycerol	1229	153.7	Silicone oil	962.8	200	38.4	0.77

phase was introduced from the two lateral channels at a flow rate of $Q_c/2$. The droplet forms as the two phases converge in the flow-focusing region. The flow rates of fluids were controlled by syringe pumps (Harvard Apparatus, PHD 2000).

A microscope (ECLIPSE Ti-CU, Nikon, Japan) coupled with a high-speed camera (Redlake Motion Pro Y-5) was used to capture the breakup process of the dispersed thread for high-viscosity droplets formation. A 12 VDC halogen lamp with a dedicated power supply (Nikon TI-PS 100W, Japan) was utilized to illuminate the channel. Frame rates used in the experiment were 8000 and 10,000 frames per second, with the exposure time of 15 μs. All images were taken when the fluid flow reached a steady state after adjusting the flow rate.

Aqueous solution of 89.5% glycerol was used as the dispersed phase, and silicone oil with various viscosities (50–200 mPa s) as the continuous phase. We defined $\lambda=\mu_d/\mu_c$ as the viscosity ratio of the dispersed phase to the continuous phase, where the subscripts "d" and "c" represent the dispersed phase and continuous phase, respectively. In the experiment, the flow rate of the dispersed phase was varied between 0.83 and 1.67 μL/min. For each fixed flow rate of the dispersed phase, we changed the flow rate of the continuous phase (from 3.33 μL/min to 100 μL/min for $\lambda=3.07$; from 1.67 μL/min to 50 μL/min for $\lambda=1.54$; and from 1.67 μL/min to 25 μL/min for $\lambda=0.77$). The Reynolds number of the continuous phase $Re_c=\rho_c w_c u_c/\mu_c$ ranges from 0.0007 to 0.16. The capillary number of the continuous phase $Ca_c=\mu_c u_c/\sigma$ ranges from 0.002 to 0.06. ρ_c, μ_c, and $u_c=Q_c/w_c^2$ are the density, viscosity and the superficial velocity of the continuous phase, respectively. w_c is the width of the microchannel, and σ the surface tension. All of our experiments were conducted at room temperature and atmospheric pressure. The contact angles of the silicone oil with various viscosities were less than 20° on both the PDMS surface and the glass surface. Meanwhile, the contact angles of the aqueous droplet and silicone oil were measured by dropping the aqueous solution on the channel surface in the presence of silicone oil, and the contact angles were found to be more than 106° and 98° with the PDMS surface and the glass surface, respectively. In our experiment, stable water-in-oil emulsion droplets could be formed. An Ubbelohde viscometer (iVisc, LAUDA, Germany) was used to characterize the viscosity of the liquids. The density of the liquids was measured by a vibrating tuber density meter (Anton Paar DMA-4500-M, Austria). The surface tension was measured using a tensiometer, by the pendant drop technique on a Tracker apparatus (Dataphysics, Germany). The properties of the experimental fluid are given in Table 2.

Results and Discussion

Two breakup types of high-viscosity thread for droplet formation

The rupture process could be divided into two categories based on the critical capillary number of the continuous phase $Ca_{c,crit}=10^{-2}$. Under low capillary numbers of the continuous phase ($Ca_c < 10^{-2}$), the fluid filament connecting the separating droplet is nearly cylindrical (Figures 2a–c) and the breakup behavior is symmetrical. This is similar to the calculated result of the breakup of the viscosity thread without the external drag,[21] here we name the process as "symmetrical rupture process." Under high capillary numbers of the continuous phase ($Ca_c > 10^{-2}$), the fluid filament is conical near-pinching (Figures 2d–f) and the breakup behavior is asymmetrical. This rupture behavior often occurs in low-viscosity droplet formation under an unconfined environment,[31] and the process is named as "asymmetrical rupture process." Moreover, both the breakup types were also observed in low-viscosity droplets formation in flow-focusing devices,[4] in which the symmetric and asymmetric rupture processes were also classified according to the critical capillary number of the continuous phase $Ca_{c,crit}=10^{-2}$. However, the inertia of the high-viscosity dispersed thread in our experiment ($10^{-4} < Re_d < 10^{-3}$) was 3–6 orders of magnitude smaller than that for the low-viscosity thread ($10^0 < Re_d < 10^2$), indicating that the driving mechanisms are different for the two types of droplet formation.

The dynamics of droplet formation for both rupture processes are presented in Figure 2. Both of the processes could be described by three stages: expansion, squeezing, and pinch-off stages. For the symmetrical rupture process (Figures 2a′–l′), after a retracting and waiting time at the expansion stage (Figures 2a′–c′), the forefront of the droplet expands in the radial and axial directions slowly until it penetrates into the outlet channel and maintains a constant radial width for a period of time. At the squeezing stage (Figures 2d′–g′), a clearly visible neck is formed under the liquid constriction and develops into a cylindrical filament gradually. Finally, the thread of the dispersed phase stretches quickly, and then both ends of the dispersed thread rupture simultaneously (Figures 2g′–i′). Subsequently, the ruptured thread retracts to form the satellite droplet due to surface tension (Figures 2j′–l′). For the asymmetrical rupture process (Figures 2a″–l″), the evolution of the dispersed thread in the first two stages is consistent with that in the symmetrical rupture process (Figures 2a″–f″), but the thread width formed in the initially squeezing stage is less than the channel width (Figure 2c″). At the pinch-off stage (Figures 2f″–h″), the shape of the thread of the dispersed phase is approximately conical (Figure 2h″). It first breaks close to the droplet and then, near the matrix. Subsequently, many satellite droplets are formed due to the multiple breakup of the ruptured thread (Figures 2i″–l″), which is quite similar to previous experimental result reported by Tjahjadi et al.[32]

In addition, the dynamics of the droplet head in both rupture processes are similar to that for the viscous droplet formed in a less viscous liquid in a microfluidic flow-focusing device.[28] As shown in Figure 3, in the early stage, the velocity of the droplet head approaches to the velocity of the dispersed phase, and then it is slightly accelerated under the action of the continuous phase until reaching the edge of the outlet channel (Figures 2b′, b″). Afterward, the flow of the continuous phase becomes significantly obstructed, and the droplet head is speeded up by the continuous phase up to the maximum speed.

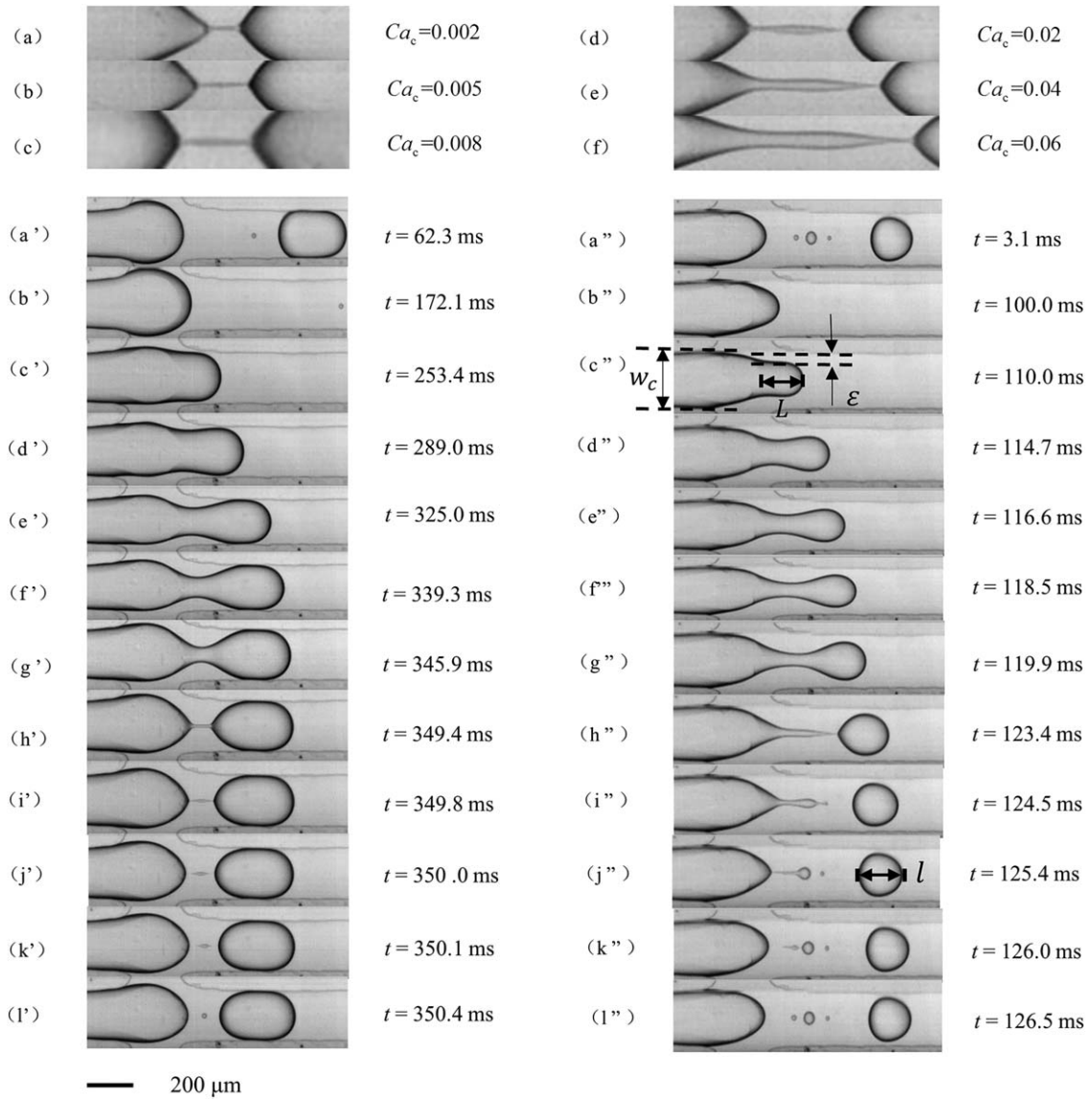

Figure 2. Dynamics of droplet formation in silicone oil in a 200μm × 200 μm flow-focusing device.

(a)–(c) Moment just before the pinch-off for the symmetrical rupture of the dispersed thread. (d)–(f) Moment just before the pinch-off for the asymmetrical rupture of the dispersed thread. (a')–(l') Symmetrical rupture process, Q_d = 1.67 μL/min Q_c = 8.33 μL/min. l/w_c = 1.70. (a″)–(l″) Asymmetrical rupture process. Q_d = 1.67 μL/min, Q_c = 66.7 μL/min. l/w_c = 0.93. μ_d = 153.7 mPa s, μ_c=50 mPa s. The time zero is set as the moment of the final pinch-off of the newly formed droplet. l represents the asymptotic axial length of the formed droplet.

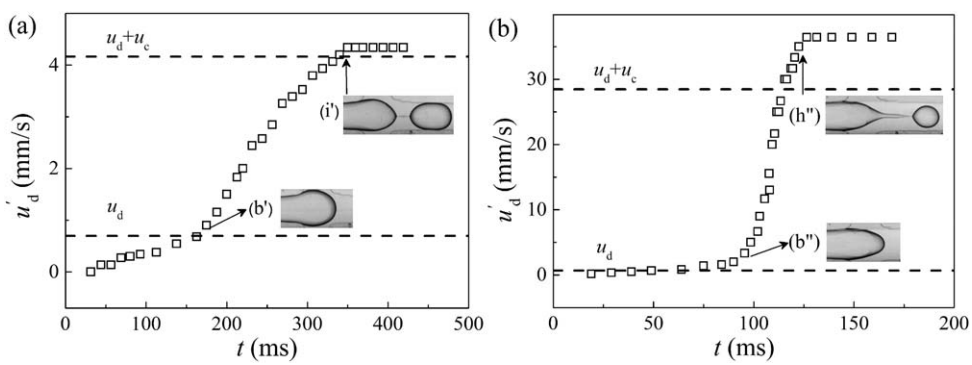

Figure 3. Head velocity of the droplet during breakup process.

(a) Symmetrical rupture process, Q_d = 1.67 μL/min, Q_c = 8.33 μL/min. l/w_c = 1.70. (b′) and (I′) are the same cases shown in the Figure 2. (b) Asymmetrical rupture process. Q_d = 1.67 μL/min, Q_c = 66.7 μL/min. l/w_c = 0.93. (b″) and (h″) are the same cases shown in the Figure 2. μ_d = 153.7 mPa s, μ_c = 50 mPa s. l represents the asymptotic axial length of the formed droplet. u_d represents superficial velocity of the dispersed phase, u_c represents superficial velocity of the continuous phase.

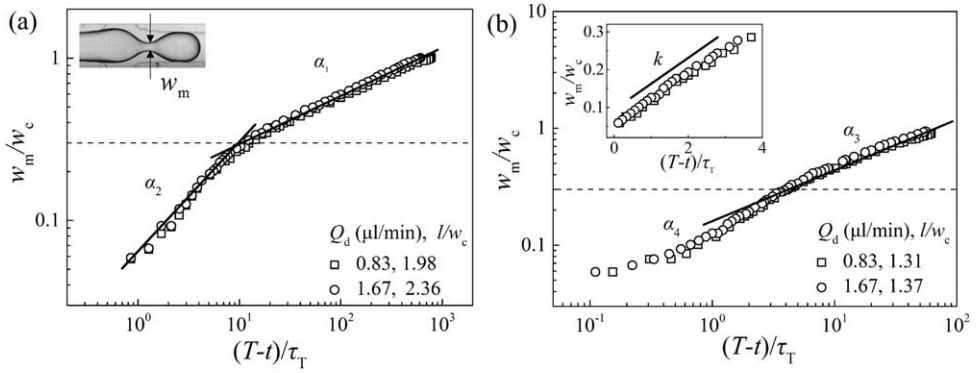

Figure 4. Evolution of the dimensionless minimum width w_m/w_c of the thread of the dispersed phase with the dimensionless remaining time $(T-t)/\tau_T$.

(a) Symmetrical rupture of the thread of the dispersed phase. $Q_c = 3.33$ μL/min. The inset shows the minimum width of the thread of the dispersed phase. (b) Asymmetrical rupture of the thread of the dispersed phase. $Q_c = 16.7$ μL/min. The inset illustrates the relationship of w_m/w_c with $(T-t)/\tau_T$ for the pinch-off stage. $\mu_d = 153.7$ mPa s, $\mu_c = 50$ mPa s. l represents the asymptotic axial length of the formed droplet.

The final velocity of droplet surpasses the superficial velocity of both phases, due to the presence of a thick lubricating film between droplets and walls.[33]

In general, the capillary number of the continuous phase plays a vital role in the rupture process under the confinement of the channel wall. As seen from Figure 2, the liquid film thickens and the rupture behavior becomes more asymmetrical with the increase of Ca_c, which is quite similar to the low-viscosity droplets forming in microchannels.[4] Consequently, the dynamics of the dispersed thread is also determined by the external fluid flow in microchannels. In comparison to the unconfined conditions, the dynamics for droplets formed in static air depends only on the viscosity of the dispersed phase.[21,31] To better understand the droplet formation process, the breakup dynamics of the dispersed thread are studied in detail in the following sections.

The breakup dynamics of dispersed thread for high-viscosity droplet formation

Scaling Law of Two Breakup Types. The breakup mechanisms of symmetrical and asymmetrical rupture processes could be investigated by analyzing the evolution of liquid–liquid interface as the neck of the dispersed phase begins to form (the second and the third stages). This method has been widely used by many researchers.[7,34] We defines w_m as the minimum width of the dispersed thread as shown in Figure 4, w_c as the width of the channel, T as the formation period of droplet, and t as the time. The minimum width of the dispersed thread w_m and the remaining time $(T-t)$ are normalized as w_m/w_c and $(T-t)/\tau_T$, respectively, where $\tau_T = \frac{\mu_d w_c}{\sigma}$ is the characteristic viscous time.[15] We focus specifically on the region of breakup dynamics of high-viscosity thread where $w_m/w_c \geq 0.05$.

Figure 4 depicts the evolution of w_m/w_c with the remaining time $(T-t)$ for both rupture processes. A conclusion could be drawn that the effect of the flow rate of the dispersed phase has no obvious effect on both breakup processes. As the neck of the dispersed phase thins along a common trajectory with varying the flow rate of the dispersed phase for a fixed flow rate of the continuous phase in either rupture process. In addition, for each rupture process, when $w_m/w_c \geq 0.3$, the dynamical behaviors are in the squeezing stage; when $w_m/w_c \leq 0.3$, the dynamical behaviors fall into the pinch-off stage. In both stages, the scaling law could be expressed as the below equation

$$w_m/w_c \propto \left(\frac{T-t}{\tau_T}\right)^{\alpha} \quad (1)$$

The variation of w_m/w_c for the symmetrical rupture process is shown in Figure 4a. In the squeezing stage, the exponent α_1 increases with the increase of the flow rate and viscosity of the continuous phase (Figures 5a, b), which coincides with the results obtained in the low-viscosity droplet formation.[4,13] In the pinch-off stage, the exponent $\alpha_2 = 0.669 \pm 0.03$ and is independent of the flow rate and viscosity of the continuous phase (Figures 5c, d), indicating a self-similar thinning process for the pinch-off stage.[35,36]

Figure 4b illustrates the evolution of w_m/w_c with the remaining time $(T-t)$ for the asymmetrical rupture process. The variation of the droplet neck in squeezing stage is consistent with that in the symmetrical rupture process, that is, the exponent α_3 increases with the increase of the flow rate and viscosity of the continuous phase (Figures 6a b). In the pinch-off stage, the exponent $\alpha_4 = 1$ and is independent of the flow rate and viscosity of the continuous phase (Figures 6c d). The pinch-off stage is also a self-similar thinning process as in the symmetrical rupture process.

As reported previously, for the final pinch-off stage of the droplet formation in unconfined systems, the power-law exponent $\alpha = 2/3$ if the inertia could balance the surface tension[9,31,37,38] and $\alpha = 1$ if the viscous force could balance the surface tension.[7,18,21] Thereupon, the difference of the scaling law in the pinch-off stage for both breakup processes in our research is possibly caused by the different driving mechanism.

The Driving Mechanism During Breakup Process. ***Squeezing stage.*** At the beginning of the squeezing stage, the forefront of the droplet partially or almost completely blocks the exit channel, leading to an increased resistance to the flow of continuous phase.[13,39] So the pressure buildup in the continuous phase squeezes the dispersed fluid, and pushes the dispersed thread into the downstream channel.[5] Therefore, in this process the forces acting on the liquid–liquid interface of the dispersed thread are: the squeezing pressure (ΔP), the shear-stress force (τ_a), the extensional stress (τ_r), and the surface tension. [14,25,26] The extensional properties of the liquid (τ_r) are also considered because the droplets are generated in elongation-dominated flow in the flow-focusing junction.[40] As illustrated in Figure 2, ε is defined as the thickness of liquid

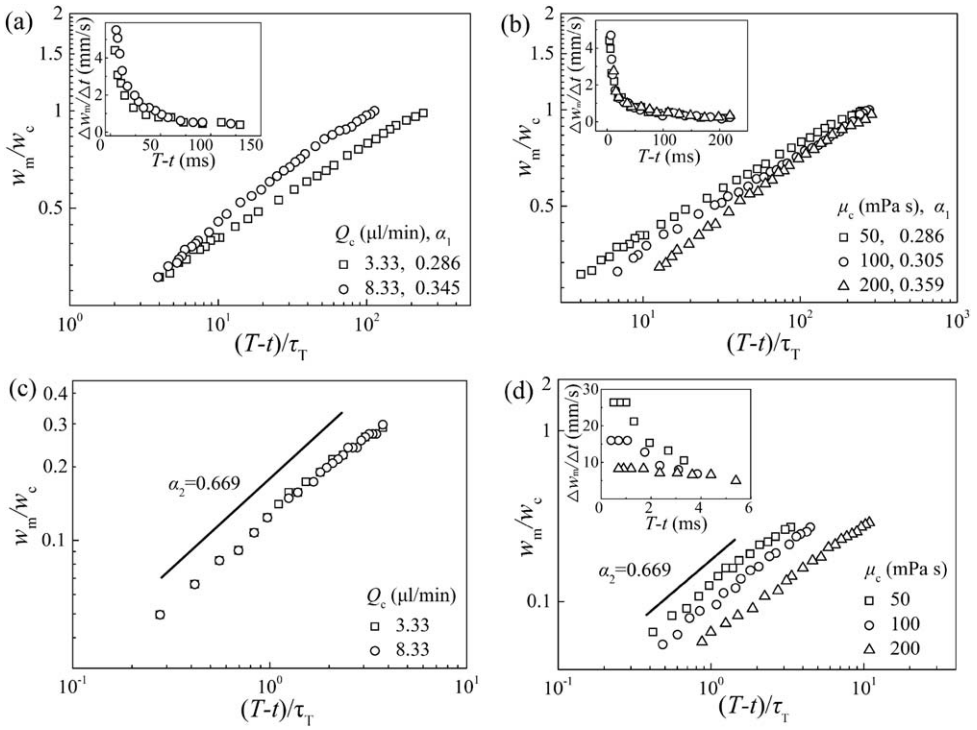

Figure 5. Scaling of the dimensionless minimum width w_m/w_c of the thread of the dispersed phase with the dimensionless remaining time $(T-t)/\tau_T$ for the symmetrical rupture process.

(a) The effect of the flow rate of the continuous phase in the squeezing stage. $Q_d = 0.83$ μL/min, $\mu_d = 153.7$ mPa·s, $\mu_c = 50$ mPa·s. (□): $Ca_c = 0.002$, $l/w_c = 1.98$; (○): $Ca_c = 0.005$, $l/w_c = 1.55$. The inset $\Delta w_m/\Delta t \sim (T-t)$ represents the thinning rate of the dispersed thread with the remaining time $(T-t)$. (b) The effect of the viscosity of the continuous phase in the squeezing stage. $Q_d = 0.83$ μL/min, $Q_c = 3.33$ μL/min, $\mu_d = 153.7$ mPa s. (□): $Ca_c = 0.002$, $l/w_c = 1.98$; (○): $Ca_c = 0.004$, $l/w_c = 1.59$; (Δ): $Ca_c = 0.007$, $l/w_c = 1.49$. Inset: $\Delta w_m/\Delta t \sim (T-t)$. (c) The effect of the flow rate of the continuous phase in the pinch-off stage. $Q_d = 0.83$ μL/min, $\mu_d = 153.7$ mPa·s, $\mu_c = 50$ mPa·s. (□): $Ca_c = 0.002$, $l/w_c = 1.98$; (○): $Ca_c = 0.005$, $l/w_c = 1.55$. (d) The effect of the viscosity of the continuous phase in the pinch-off stage. $Q_d = 0.83$ μL/min, $Q_c = 3.33$ μL/min, $\mu_d = 153.7$ mPa·s. (□): $Ca_c = 0.002$, $l/w_c = 1.98$; (○): $Ca_c = 0.004$, $l/w_c = 1.59$; (Δ): $Ca_c = 0.007$, $l/w_c = 1.49$. Inset: $\Delta w_m/\Delta t \sim (T-t)$. l represents the asymptotic axial length of the formed droplet.

film between the interface and the wall of channel, h is the depth of the channel, and L is the length of the head of the droplet.

The squeezing pressure could be calculated by the pressure drop of the continuous phase flowing though the fluid film. In the experiment, the thickness of the liquid film between droplets and walls is in the range of $\varepsilon/w_c < 26\%$, the squeezing pressure could be expressed as[25,26]

$$\Delta P \approx \mu_c Q_c L/(h\varepsilon^3) \tag{2}$$

The shear force could be estimated as $\tau_a \approx \mu_c u_g/(2\varepsilon)$, where $u_g = Q_c/A$ is the velocity of the continuous phase flowing through the gap between the liquid–liquid interface and the wall of the channel, and $A = w_c^2 - \frac{\pi}{4}(w_c - 2\varepsilon)^2$ is the cross-sectional area of the gap between the liquid–liquid interface and the wall of the channel.[27] So the shear force could be expressed as

$$\tau_a = \frac{\mu_c Q_c}{2\varepsilon[w_c^2 - 0.785(w_c - 2\varepsilon)^2]} \tag{3}$$

The extensional stress for the continuous phase is $\tau_r = \mu_{e,c}\dot{\varepsilon}_c$, where $\mu_{e,c} = 3\mu_c$ is the extensional viscosity and $\dot{\varepsilon}_c \approx Q_c/w_c^3$ is the extensional strain rate,[14,41] Thus, the extensional stress could be expressed as

$$\tau_r = \mu_{e,c}\dot{\varepsilon}_c \approx 3\mu_c Q_c/w_c^3 \tag{4}$$

The surface tension could be given by the Laplace pressure jump between the head and the neck of the emerging droplet, as shown below[25,26]

$$\Delta P_L = \sigma(r_a^{-1} + r_r^{-1}) \tag{5}$$

where r_a is the axial curvature and r_r is the radial curvature. At the beginning of the neck formation, the Laplace pressure at the head of the dispersed thread is $P_L^{up} \approx -\sigma(2/w_c + 2/h) \approx -4\sigma/w_c$, and the Laplace pressure at the neck of the dispersed thread is $P_L^{up} \approx 2\sigma/w_c$. Therefore, the Laplace pressure jump is $\Delta P_L \approx -2\sigma/w_c$.

At the beginning of the squeezing stage, the squeezing pressure, shear force, and extensional stress can all resist the surface tension and control the evolution of the thread of the dispersed phase. To identify the leading driving force in this stage, we compare the magnitudes of these forces for the two breakup processes at the initial droplet neck formation stage (Figures 2c′, c″). For the symmetrical rupture process ($\varepsilon/w_c < 8\%$), $\Delta P \gg \tau_a$, $\Delta P \geq 2100$Pa, and $\tau_r = [0, 4.2]$ Pa. For the asymmetrical rupture process ($8\% < \varepsilon/w_c < 26\%$), $\Delta P = [500-3000]$Pa, $\tau_a = [16, 27]$Pa, and $\tau_r = [2, 32]$Pa. Consequently, we can expect that the variation of the droplet neck in the two breakup processes is mainly driven by the squeezing pressure in the squeezing stage.[25]

The dynamics will change from the squeezing stage to the pinch-off stage after the thread width becomes smaller than the critical value $w_m/w_c = 0.3$. It is interesting to note that the

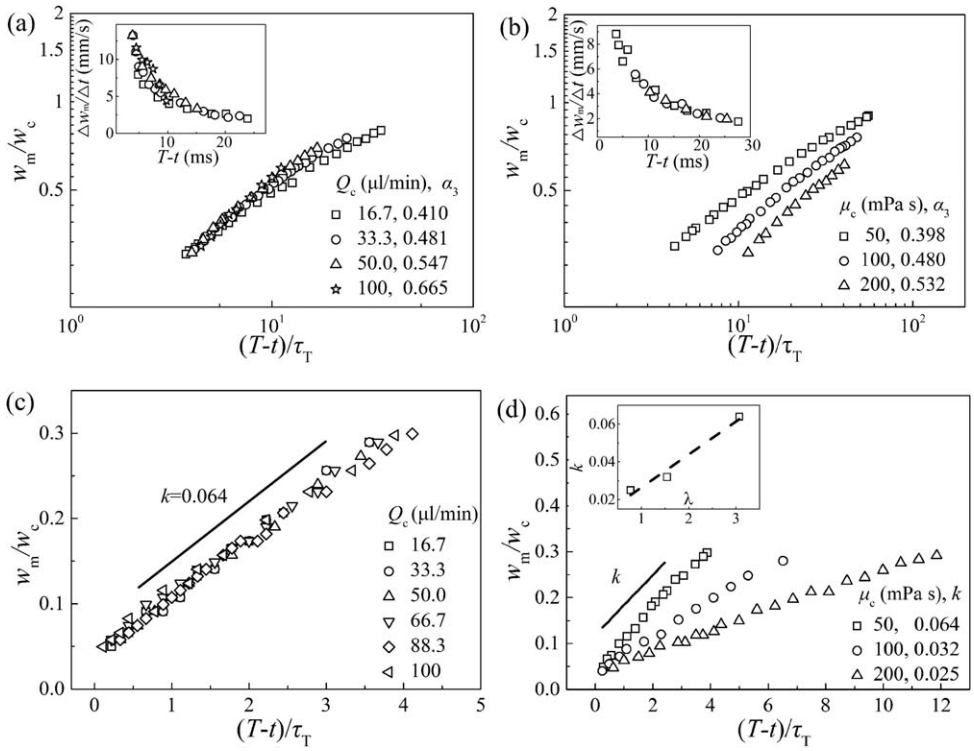

Figure 6. Scaling of the dimensionless minimum width w_m/w_c of the thread of the dispersed phase with the dimensionless remaining time $(T-t)/\tau_T$ for the asymmetrical rupture process.

(a) The effect of the flow rate of the continuous phase in the squeezing stage. $Q_d = 0.83$ μL/min, $\mu_d = 153.7$ mPa·s, $\mu_c = 50$ mPa·s. (□): $Ca_c = 0.010$, $l/w_c = 1.31$; (○): $Ca_c = 0.020$, $l/w_c = 1.12$; (Δ): $Ca_c = 0.030$, $l/w_c = 1.00$; (⋆): $Ca_c = 0.061$, $l/w_c = 0.83$. The inset $\Delta w_m/\Delta t \sim (T-t)$ represents the thinning rate of the dispersed thread with the remaining time $(T-t)$. (b) The effect of the viscosity of the continuous phase in the squeezing stage. $Q_d = 0.83$ μL/min, $Q_c = 16.7$ μL/min, $\mu_d = 153.7$ mPa·s. (□): $Ca_c = 0.010$, $l/w_c = 1.31$; (○): $Ca_c = 0.019$, $l/w_c = 1.14$; (Δ): $Ca_c = 0.036$, $l/w_c = 0.88$. Inset: $\Delta w_m/\Delta t \sim (T-t)$. (c) The effect of the flow rate of the continuous phase in the pinch-off stage. $Q_d = 0.83$ μL/min, $\mu_d = 153.7$ mPa·s, $\mu_c = 50$ mPa·s. (□): $Ca_c = 0.010$, $l/w_c = 1.31$; (○): $Ca_c = 0.020$, $l/w_c = 1.12$; (Δ): $Ca_c = 0.030$, $l/w_c = 1.00$. (▽): $Ca_c = 0.041$, $l/w_c = 0.91$; (◇): $Ca_c = 0.051$, $l/w_c = 0.87$; (◁): $Ca_c = 0.061$, $l/w_c = 0.83$. (d) The effect of the viscosity of the continuous phase in the pinch-off stage. $Q_d = 0.83$ μL/min, $Q_c = 16.7$ μL/min, $\mu_d = 153.7$ mPa·s. (□): $Ca_c = 0.010$, $l/w_c = 1.31$; (○): $Ca_c = 0.019$, $l/w_c = 1.14$; (Δ): $Ca_c = 0.036$, $l/w_c = 0.88$. The inset $k \sim \lambda$ illustrates the relationship of k with the viscosity ratio of the fluids λ in the pinch-off stage. l represents the asymptotic axial length of the formed droplet.

critical value is irrelevant to the breakup type, indicating that the transformation is not affected by the capillary number of continuous phase, but is determined by the intrinsic properties of the dispersed thread. Here we introduce the Ohnesorge number $Oh=\mu/\sqrt{\rho\sigma w_m}$, which captures the ratio of viscous forces to capillary forces, to illustrate the properties of the dispersed thread. Figure 7 displays the variation of the local Ohnesorge number $Oh=\mu_d/\sqrt{\rho_d\sigma w_m}$ of the dispersed phase with the remaining time. Although the variation of Oh with the remaining time $(T-t)$ is different in the both rupture processes, the value of Oh is in the same order of magnitude for the two processes. In addition, when $w_m/w_c > 0.3$, the Ohnesorge number changes very slowly. When $w_m/w_c < 0.3$, the Ohnesorge number increases quickly. Therefore, it suggests that the transformation from squeezing to pinch-off stage would occur when the viscous force of the dispersed phase becomes important and Oh greater than a certain critical value.

Pinch-off stage. In the pinch-off stage, the Rayleigh–Plateau instability eventually sets in, so that the viscous force, inertial force, and the surface tension control the evolution of the dispersed thread.[7] The relative importance of the three forces can be characterized by the Reynolds number (the relative importance of inertial force to viscous force) and the Weber number (the relative importance of inertial force to surface tension). The local Reynolds number of the continuous phase and the dispersed phase can be defined respectively as

$$Re_{c,local}=\rho_c w_m w'_m/\mu_c \quad (6)$$

$$Re_{d,local}=\rho_d w_m u_d/\mu_d \quad (7)$$

The local Weber number of the continuous phase and the dispersed phase can be defined respectively as

$$We_{c,local}=\rho_c w_m w'^2_m/\sigma \quad (8)$$

$$We_{d,local}=\rho_d w_m u'^2_d/\sigma \quad (9)$$

Where w'_m is the decrement rate at the minimum width of the neck of the dispersed thread, and u'_d is the velocity of the droplet head of the dispersed phase. In this stage, the four dimensionless numbers in the symmetric rupture process are, respectively, in the same order of magnitude with the corresponding ones in the asymmetric rupture process. In general, $Re_c < 0.04$, $Re_d < 0.08$, $We_c < 3\times10^{-4}$, and $We_d < 6\times10^{-3}$. Therefore, the inertial force is insignificant. Furthermore, viscous effects have an important impact on the evolution of the neck due to the large viscosity of both fluids. Accordingly, the neck thinning is controlled jointly by surface tension and the viscous forces of both fluids.

In the asymmetrical rupture process, the profile shape of the dispersed thread is conical and the variation of the minimum width of the dispersed thread with the remaining time could be described by a linear relationship. These results are very similar to the dynamics of Stokes regime in macroscale.[7,11,42] The evolution of the liquid–liquid interface is the result of the

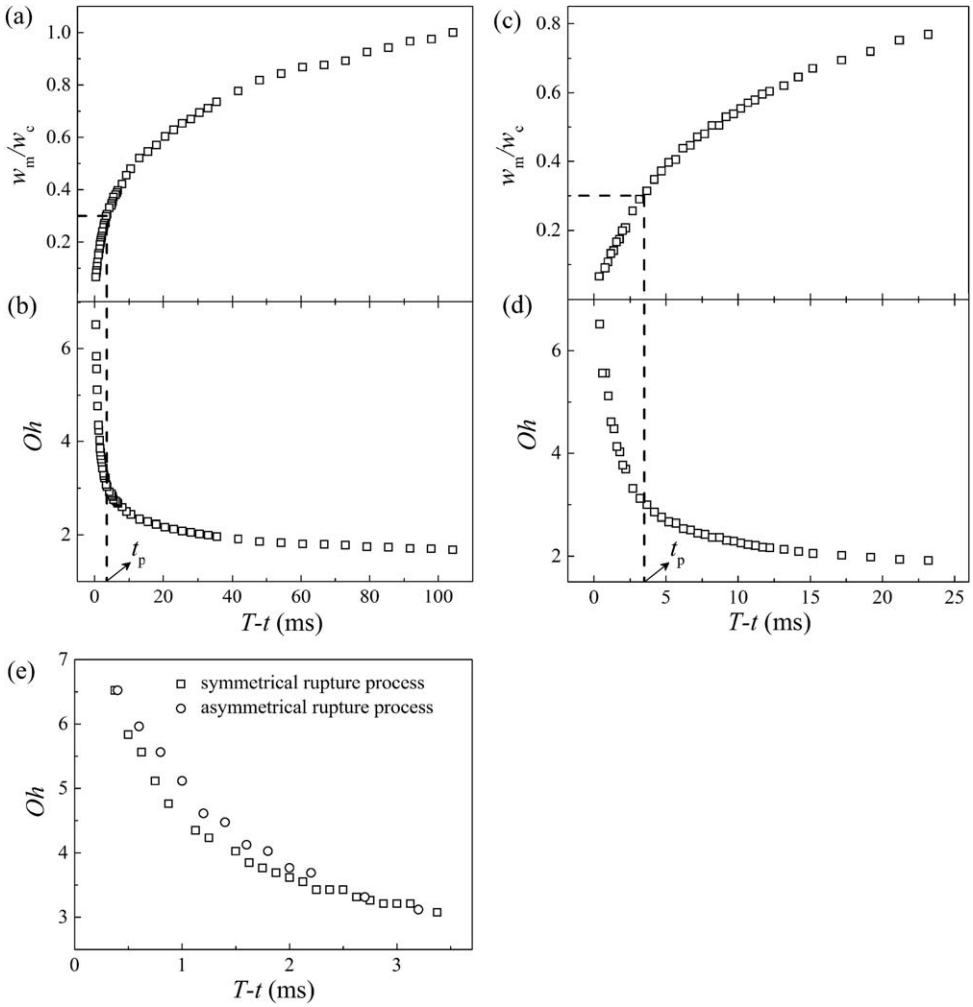

Figure 7. Evolution of the dimensionless minimum width w_m/w_c of the thread of the dispersed phase and *Oh* with the remaining time ($T-t$).

(a) Evolution of w_m/w_c with ($T-t$) for the symmetrical rupture process. $Q_d = 0.83$ μL/min, $Q_c = 8.33$ μL/min. (b) The computed *Oh* for the same case shown in (a). (c) Evolution of w_m/w_c with ($T-t$) for the asymmetrical rupture process. $Q_d = 0.83$ μL/min, $Q_c = 33.3$ μL/min. (d) The computed *Oh* for the same case shown in (c). (e) The computed *Oh* in the pinch-off stage for the same cases shown in (a) and (c). t_p is the transformation time from the squeezing stage to the pinch-off stage. $\mu_d = 153.7$ mPa·s, $\mu_c = 50$ mPa·s.

asymptotic balance between surface tension and the viscous forces of both phases. Nevertheless, in the symmetrical rupture process, the shape of the dispersed thread is quasicylindrical and the variation of the droplet neck with the remaining time is a power-law relationship with an exponent approaching to 2/3. The scaling law is similar to the low-viscosity droplet formation in unconfined condition, in which the force balance between the inertia and surface tension results in a conical shape of the dispersed thread near the pinch-off. However, in the symmetrical rupture process in our experiment, the high viscous force (*Oh* number for the dispersed phase is in the range of $3 < Oh < 7$) and the low inertia force ($Re_d \ll 1$, $Re_c \ll 1$) generate a quasicylindrical shape in the last stage, indicating a totally different pinch-off mechanism. Recently, Castrejón-Pita et al.[43] also discovered a power-law relationship with $\alpha = 2/3$ between the dimensionless minimum neck width and the remaining time in a high-viscosity liquid ($Oh = 1.81$) under macroscopic scale by numerical simulation. It is worthy of note that the power-law relationship found by Castrejón-Pita et al.[43] was obtained for the dimensionless minimum neck width varying from 0.001 to 0.04. However, for the high-viscosity dispersed thread pinch-off in this study, the power-law relationship was applied to the dimensionless minimum neck width in the range of 0.05 to 0.3. For the breakup of the high-viscosity dispersed thread in the microchannel, the mechanism resulted in the power law relationship between the minimum neck width and the remaining time with exponent 2/3 remains unknown. Nevertheless, the viscous stress in the symmetrical rupture process is small than that in the asymmetrical rupture process due to the small capillary number of the continuous phase Ca_c and the *Oh* number (as shown in Figure 7e) in the symmetrical one. Therefore, the viscous force is unequal to the surface tension in the pinch-off stage of the symmetrical rupture process. Moreover, the power-law relationship between the minimum width of the dispersed thread and the remaining time demonstrates that the breaking of the dispersed neck is accelerated gradually under the driven of surface tension.

In addition, the axial velocity v of the filament dominates the local strain field which determines the evolution of the dispersed thread.[7] To better understand the driving mechanism of both breakup processes, we analyze the axial velocity v_{w_m} at

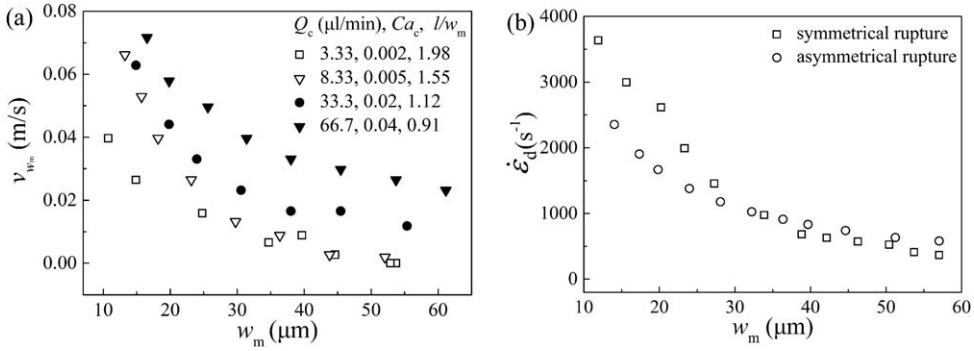

Figure 8. (a) Evolution of the axial velocity v_{w_m} with the minimum width w_m of the thread of the dispersed phase. The hollow symbols indicate the symmetrical rupture process; the solid symbols indicate the asymmetrical rupture process. *l* represents the asymptotic axial length of the formed droplet. (b) Evolution of the extensional strain rate $\dot{\varepsilon}_d = -(2/w_m)dw_m/dt$ with w_m for the symmetrical rupture process and asymmetrical rupture process. For the symmetrical rupture process, $Q_d = 0.83$ μL/min, $Q_c = 8.33$ μL/min. For the asymmetrical rupture process, $Q_d = 0.83$ μL/min, $Q_c = 33.3$ μL/min. μ_d = 153.7 mPa·s, μ_c = 50 mPa·s.

the point of the minimum width of the dispersed thread in the pinch-off stage. The axial velocity v_{w_m} could be calculated by $\Delta l/\Delta t$, where Δl is obtained by tracing the moving distance of the point of the minimum width of the dispersed thread near the droplet within the time Δt.

Figure 8a shows the variation of the axial velocity v_{w_m} with the minimum width w_m of the dispersed thread. For both rupture processes, v_{w_m} increases with the decrease of w_m, which is similar to the simulation result of Lister and Stone.[7] Moreover, since the scaling law in this stage is unchanged with the remaining time for the both rupture processes, it means that the increase of v_{w_m} with the remaining time only plays the role to transport fluid, but has a negligible effect on the driving mechanism of the neck thinning. Generally, the axial velocity v_{w_m} is small in the symmetrical rupture process, which is not strong enough to create a tug-of-war effect in the thread as proposed by Lister and Stone,[7] therefore, the interface would be cylindrical. However, in the asymmetrical rupture process, the larger axial velocity v_{w_m} could generate a tug-of-war effect, Due to this effect, two cones will form in the pinch-off region. The conical region of the forming droplet pulls the pinching neck toward itself and stretches out the cone on the dispersed thread, which result in a nonlocal velocity component.[7] Here, the nonlocal velocity component represents the contribution to the axial velocity v in the intermediate region between the two cones, and v increases with the decrease of the minimum width of the dispersed thread.[7]

It has been known that the local deformation in the Stokes regime is achieved by the self-similar strain field,[7] so we assume that the difference in the shape and the scaling law between the two rupture processes might be caused by the disparity of the strain field. The extensional strain rate could be expressed as[14,44]

$$\dot{\varepsilon}_d = -(2/w_m)dw_m/dt \tag{10}$$

Figure 8b illustrates the variation of the extensional strain rate $\dot{\varepsilon}_d$ with the minimum width w_m of the dispersed thread. From the figure, it could be seen that $\dot{\varepsilon}_d$ increases with the decrease of w_m. In addition, the obvious difference in $\dot{\varepsilon}_d$ before pinch-off ($w_m < 30$ μm) indicates the disparity of the strain field between the two breakup processes, which results in differences in the local interface deformation in the two breakup processes. It is the flow of the external fluid and its properties that result in the difference in the strain fields between the two rupture processes. Therefore, we investigate the effects of the flow rates and viscosity of the continuous phase on the breaking rate and the dynamical behaviors of both rupture processes in the following section.

Effects on the Rupture Process. ***Influences on the symmetrical rupture process.*** Figure 5 describes the quantitative influence of the flow rate Q_c and viscosity μ_c of the continuous phase on the variation of the dispersed thread for the symmetrical rupture process. Figures 5a, b illustrate the effects on the squeezing stage. It could be seen that the exponent α_1 increases with the increase of the flow rate and viscosity of the continuous phase. In addition, as shown in the inset of the Figure 5a, a slight reduction in the thinning rate of the dispersed thread could be clearly seen with the increase of the flow rate of the continuous phase under the driven of squeezing pressure. Obviously, this observed effect on collapse velocity of the high-viscosity thread with varying the flow rate of the continuous phase is not remarkable as the experimental research with low-viscosity liquid.[45] This phenomenon could be attributed to the high stretching stress in the high-viscosity dispersed thread, which delays the rupture process.[5] At the same time, From the inset of the Figure 5b, it could be easily found that the thinning rate of the breakup process is almost not affected by the viscosity of the continuous phase, which indicates again that the change of the dispersed thread in this stage is dominated by the squeezing pressure.[8,46]

In the pinch-off stage, the exponent $\alpha_2 = 0.669 \pm 0.03$, which is independent of the flow rate and viscosity of the continuous phase, as seen in the Figures 5c, d. Additionally, the flow rate of the continuous phase has no obvious effect on the thinning of the neck. Therefore, the extensional strain field at the point of breakup is hardly affected by the flow rate of the continuous phase. For the symmetrical rupture process, as shown in Figure 8a, the axial velocity v_{w_m} increases with the flow rate of the continuous phase Q_c. The shape of filament is approximately cylindrical and the length also grows with increasing Q_c (Figures 9a, b). Therefore, the axial velocity v_{w_m} and the state of the dispersed thread vary with the increase of the flow rate of the continuous phase, but those changes have no effects on the neck thinning. Conversely, the collapse velocity of the dispersed phase decreases with the increase of the viscosity of the continuous phase, as seen in the inset of Figure 5d. This phenomenon could be attributed to the viscous drag during the breakup process.[18,30,47]

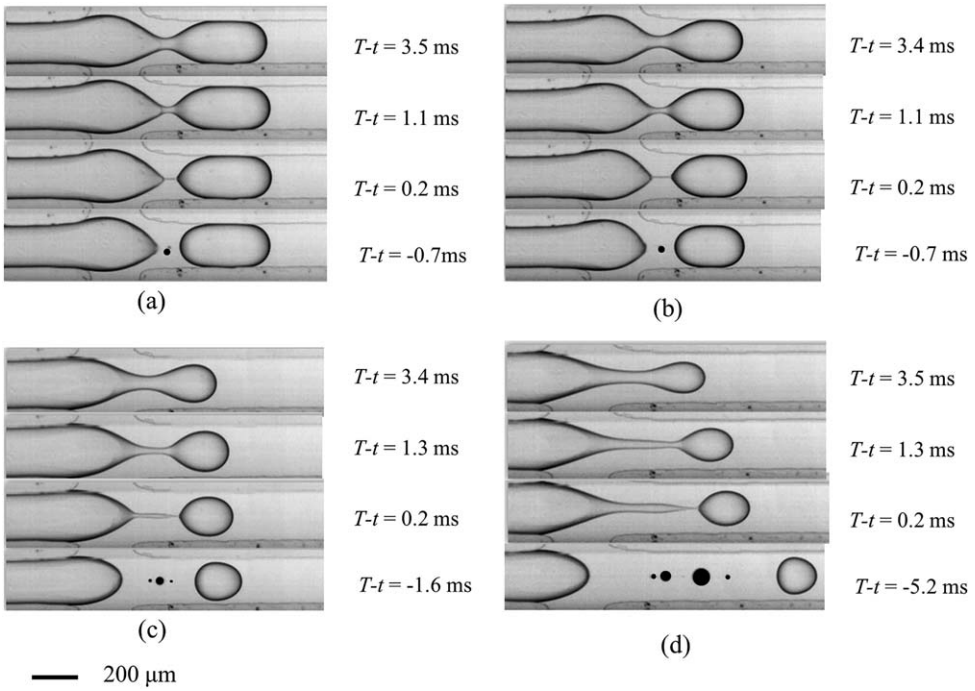

Figure 9. Details of the neck rupturing and the formation of satellite droplets.

(a) and (b) Symmetrical rupture process. (a) $Q_d = 0.83$/min, $Q_c = 3.33$ μL/min, $l/w_c = 1.98$. (b) $Q_d = 0.83$ μL/min $Q_c = 8.33$ μL/min, $l/w_c = 1.55$. (c) and (d) Asymmetrical rupture process. (c) $Q_d = 0.83$ μL/min, $Q_c = 50.0$ μL/min, $l/w_c = 1.00$. (d) $Q_d = 0.83$ μL/min $Q_c = 100$ μL/min, $l/w_c = 0.83$. $\mu_d = 153.7$ mPa·s, $\mu_c = 50$ mPa·s. The solid symbols in black indicate the satellite droplets. l represents the asymptotic axial length of the formed droplet.

In the pinch-off stage, the power-law exponent $\alpha_2 = 0.669 \pm 0.03$, and the thinning of the dispersed thread is only related to the viscosity of the continuous phase. Thus, the scaling law could be expressed as $w_m/w_c = A\left(\frac{T-t}{\tau_T}\right)^{0.669}$ (when $\mu_c = 50$mPa·s, $A = 0.123$; when $\mu_c = 100$mPa·s, $A = 0.103$; and when $\mu_c = 200$mPa·s, $A = 0.058$).

Influences on the asymmetrical rupture process. Figure 6 describes the quantitative influence of the flow rate Q_c and viscosity μ_c of the continuous phase on the variation of the dispersed thread for the asymmetrical rupture process. Figures 6a, b illustrate the effects on the squeezing stage. As with the symmetrical rupture process, the exponent α_3 increases with the increase of the flow rate and viscosity of the continuous phase. In addition, as shown in the inset of Figures 6a, b, the thinning rate of the dispersed thread is almost independent of the flow rate of the continuous phase and it remains unaffected by the viscosity of the continuous phase.

In the pinch-off stage, the exponent $\alpha_4 = 1$ is independent of the flow rate and viscosity of the continuous phase, as seen in the Figures 6c, d. Furthermore, the flow rate of the continuous phase also has no obvious effect on the neck thinning. These results are similar to the symmetrical rupture process in this stage. However, for the asymmetrical rupture process, the thread becomes longer and the asymmetry of the liquid–liquid interface gets stronger with the increase of the flow rate of the continuous phase. Meanwhile, more satellite droplets will be formed as well (Figures 9c, d).

As shown in the Figure 6d, the collapse velocity of the dispersed thread decreases with the increase in viscosity of the continuous phase due to the viscous drag. In this stage, the dynamical behavior of the dispersed thread is similar to that in Stokes regime in the macroscale. Stone et al.[7] suggested that the variation of the dispersed thread in Stokes regime could be scaled as $w_m = k(\lambda)\frac{\sigma}{\mu_d}(T-t)$, where k is a dimensionless function depending on the viscosity ratio of the fluids λ. The values of k calculated in our experiment, $k = 0.064$ for $\lambda = 3.07$, $k = 0.032$ for $\lambda = 1.54$, and $k = 0.025$ for $\lambda = 0.77$, are close to both the results of $k = 0.031 \pm 0.008$ obtained experimentally[11] and $k = 0.0335$ by simulation[7] when $\lambda = 1$. The correlation $k \propto \lambda^{-0.53 \pm 0.05}$ was obtained in previous studies by varying the viscosity of the dispersed phase.[11,42] However, in this work, an opposite trend between k and λ was attained by changing the viscosity of the continuous phase. According to present experimental result, a linear relationship $k = 0.0175\lambda + 0.0089$ was obtained, as shown in the inset of the Figure 6d. Recently, Arratia et al.[14] investigated the process of the high-viscosity filament breakup in another high-viscosity fluid. This study assumed a stress balance between radial stress and the Laplace pressure $\mu_{e,d}\dot{\varepsilon} = \sigma/w_c$ without considering of the viscous force of the external fluid. Therefore, the high-viscosity filament thins linearly as the below equation

$$w_m(t) = -1/2(\sigma/\mu_{e,d})(T-t) \tag{11}$$

The value of k obtained from Eq. 11 is $k = 0.17$, which is larger than the value obtained in our experiment. This indicates that the viscous stress of the continuous phase cannot be ignored, and the variation of the thread of the dispersed phase is resulted from the combined effect of the viscous stresses of both phases and the surface tension.

It is noteworthy that the evolution of the dispersed phase changes with the variation of the flow rate and viscosity of the continuous phase. Additionally, the transformation from symmetrical rupture process to asymmetrical rupture process occurs in low flow rate of the continuous phase when high-viscosity fluids are used as the continuous phase. In general, the effects of the flow rate and viscosity of the continuous

phase cause the transformation to occur at a critical capillary number $Ca_{c,crit}=10^{-2}$ for highly viscous droplets forming in another immiscible viscous fluid under the confinement of the microchannel.

Conclusions

In this work, the breakup mechanism of high-viscosity thread for droplet formation in other immiscible viscous fluids in a flow-focusing device is studied systematically. Symmetrical and asymmetrical rupture processes of the dispersed thread are observed during the drop formation process. Generally, the breakup process involves two stages: squeezing stage and pinch-off stage. In the squeezing stage, squeezing pressure plays a leading role in the neck thinning for both rupture processes. The collapse rate is not significantly affected by the flow rate and viscosity of the continuous phase. In the pinch-off stage, the variation in the thinning of the dispersed neck is due to the combined effects of the viscous stresses of both phases and surface tension. The flow rate of the continuous phase has no obvious impact on the collapse rate of the dispersed thread in this stage. Nevertheless, under the effect of the viscous drag, the breaking rate decreases with increasing the viscosity of the continuous phase. Specifically, under the effects of the confinement of the channel and the flow of the external fluid, the differences between the two rupture processes mainly stem from the different strain fields at the point of detachment in the pinch-off stage. This study provides the foundation for further theoretical and experimental investigations on the high-viscosity droplet formation and breakup processes for soft matter synthesis and design of microfluidic devices.

Acknowledgments

The financial supports for this project from the National Natural Science Foundation of China (21276175, 91434204, 21106093), the Tianjin Natural Science Foundation (13JCQNJC05500), the aid of Opening Project of State Key Laboratory of Chemical Engineering (No. SKL-ChE-13T04), and the Program of Introducing Talents of Discipline to Universities (B06006) are gratefully acknowledged.

Notations

A = coefficient of power law function
h = depth of the channel, μm
k = coefficient of the linear function
l = asymptotic axial length of the formed droplet, μm
L = length of the drop head, μm
P_L = Laplace pressure, Pa
ΔP = squeezing pressure, Pa
ΔP_L = Laplace pressure jump, Pa
Q_d = volumetric flow rate of dispersed phase, μL·min^{-1}
Q_c = volumetric flow rate of continuous phase, μL·min^{-1}
r_a = radius of the axial curvature
r_r = radius of the radial curvature
T = droplet formation period, μs
t = time, μs
u = superficial velocity of liquid, m·s^{-1}
u'_d = velocity of the droplet head of the dispersed phase, m·s^{-1}
v = e filament, m·s^{-1}
w_c = width of the channel, μm
w_m = minimum width of the dispersed thread, μm
w_m = e dispersed thread, m·s^{-1}

Greek letters

α = exponent for power-law relationship
ε = thickness of liquid film, μm
$\dot{\varepsilon}$ = ate, s^{-1}
λ = Viscosity ratio of disperse phase to continuous phase ($\lambda=\mu_d/\mu_c$)
μ = viscosity of liquid, mPa·s
ρ = density of liquid, kg·m^{-3}
σ = surface tension of liquid, mN·m^{-1}
τ_T = viscocapillary time, μs
τ_a = shear stress, Pa
τ_r = extensional stress, Pa

Dimensionless groups

Ca = capillary number ($Ca = u\mu/\sigma$)
Oh = Ohnesorge number ($Oh = \mu/(\rho\sigma w_c)^{1/2}$)
Re = Reynolds number ($Re = \rho w_c u/\mu$)
We = Weber number ($We = CaRe = \rho w_c u^2/\sigma$)

Subscripts

c = continuous phase
crit = critical capillary number
d = dispersed phase
e = extensional viscosity
g = the modified continuous phase velocity
up = neck of the droplet
tip = head of the droplet

Literature Cited

1. Carrick C, Larsson PA, Brismar H, Aidun C, Wågberg L. Native and functionalized micrometre-sized cellulose capsules prepared by microfluidic flow focusing. *RSC Adv*. 2014;4:19061–19067.
2. Duncanson WJ, Zieringer M, Wagner O, Wilking JN, Abbaspourrad A, Haag R, Weitz DA. Microfluidic synthesis of monodisperse porous microspheres with size-tunable pores. *Soft Matter*. 2012;8:10636.
3. Utada AS, Lorenceau E, Link DR, Kaplan PD, Stone HA, Weitz DA. Monodisperse double emulsions generated from a microcapillary device. *Science*. 2005;308:537–541.
4. Carrier O, Dervin E, Funfschilling D, Li HZ. Formation of satellite droplets in flow-focusing junctions: volume and neck rupture. *Microsys Technol*. 2015;21:499–507.
5. Nie ZH, Seo MS, Xu SQ, Lewis PC, Mok M, Kumacheva E, Whitesides GM, Garstecki P, Stone HA. Emulsification in a microfluidic flow-focusing device: effect of the viscosities of the liquids. *Microfluid Nanofluidics*. 2008;5:585–594.
6. Xu Q, Hashimoto M, Dang TT, Hoare T, Kohane DS, Whitesides GM, Langer R, Anderson DG. Preparation of monodisperse biodegradable polymer microparticles using a microfluidic flow-focusing device for controlled drug delivery. *Small*. 2009;5:1575–1581.
7. Lister JR, Stone HA. Capillary breakup of a viscous thread surrounded by another viscous fluid. *Phys Fluids*. 1998;10:2758–2764.
8. Garstecki P, Stone HA, Whitesides GM. Mechanism for flow-rate controlled breakup in confined geometries: a route to monodisperse emulsions. *Phys Rev Lett*. 2005;94:164501.
9. Chen AU, Notz PK, Basaran OA. Computational and experimental analysis of pinch-off and scaling. *Phys Rev Lett*. 2002;88:174501.
10. Rothert A, Richter R, Rehberg I. Transition from symmetric to asymmetric scaling function before drop pinch-off. *Phys Rev Lett*. 2001;87:084501.
11. Cohen I, Brenner MP, Eggers J, Nagel SR. Two fluid drop snap-off problem-experiments and theory. *Phys Rev Lett*. 1999;83:1147–1150.
12. Dollet B, van Hoeve W, Raven J-P, Marmottant P, Versluis M. Role of the channel geometry on the bubble pinch-off in flow-focusing devices. *Phys Rev Lett*. 2008;100:034504.
13. Fu T, Wu Y, Ma Y, Li HZ. Droplet formation and breakup dynamics in microfluidic flow-focusing devices: from dripping to jetting. *Chem Eng Sci*. 2012;84:207–217.
14. Arratia PE, Gollub JP, Durian DJ. Polymeric filament thinning and breakup in microchannels. *Phys Rev E*. 2008;77:036309.
15. Steinhaus B, Shen AQ, Sureshkumar R. Dynamics of viscoelastic fluid filaments in microfluidic devices. *Phys Fluids*. 2007;19:073103.
16. Brenner MP, Eggers J, Joseph K, Nagel SR, Shi XD. Breakdown of scaling in droplet fission at high Reynolds numbers. *Phys Fluids*. 1997;9:1573–1590.
17. Yildirim OE, Basaran OA. Deformation and breakup of stretching bridges of Newtonian and shear-thinning liquids: comparison of one- and two-dimensional models. *Chem Eng Sci*. 2001;56:211–233.

18. Burton JC, Waldrep R, Taborek P. Scaling and instabilities in bubble pinch-off. *Phys Rev Lett*. 2005;94:184502.
19. Doshi P, Cohen I, Zhang WW, Siegel M, Howell P, Basaran OA, Nagel SR. Persistence of memory in drop breakup: the breakdown of universality. *Science*. 2003;302:1185–1188.
20. Zhang XG, Basaran OA. An experimental study of dynamics of drop formation. *Phys Fluids*. 1995;7:1184–1203.
21. Papageorgiou DT. On the breakup of viscous liquid threads. *Phys Fluids*. 1995;7:1529–1544.
22. Eggers J. Universal pinching of 3D axisymmetric free-surface flow. *Phys Rev Lett*. 1993;71:3458–3460.
23. Roché M, Aytouna M, Bonn D, Kellay H. Effect of surface tension variations on the pinch-off behavior of small fluid drops in the presence of surfactants. *Phys Rev Lett*. 2009;103:264501.
24. Zhang WW, Lister JR. Similarity solutions for capillary pinch-off in fluids of differing viscosity. *Phys Rev Lett*. 1999;83:1151–1154.
25. Garstecki P, Fuerstman MJ, Stone HA, Whitesides GM. Formation of droplets and bubbles in a microfluidic T-junction-scaling and mechanism of break-up. *Lab Chip*. 2006;6:437–446.
26. Christopher GF, Noharuddin NN, Taylor JA, Anna SL. Experimental observations of the squeezing-to-dripping transition in T-shaped microfluidic junctions. *Phys Rev E*. 2008;78:036317.
27. Xu JH, Li SW, Tan J, Luo GS. Correlations of droplet formation in T-junction microfluidic devices: from squeezing to dripping. *Microfluid Nanofluidics*. 2008;5:711–717.
28. Cubaud T, Mason TG. Capillary threads and viscous droplets in square microchannels. *Phys Fluids*. 2008;20:053302.
29. Van Hoeve W, Dollet B, Versluis M, Lohse D. Microbubble formation and pinch-off scaling exponent in flow-focusing devices. *Phys Fluids*. 2011;23:092001.
30. Lu Y, Fu T, Zhu C, Ma Y, Li HZ. Pinch-off mechanism for Taylor bubble formation in a microfluidic flow-focusing device. *Microfluid Nanofluidics*. 2014;16:1047–1055.
31. Day RF, Hinch EJ, Lister JR. Self-similar capillary pinchoff of an inviscid fluid. *Phys Rev Lett*. 1998;80:704–707.
32. Tjahjadi M, Stone HA, Ottino JM. Satellite and subsatellite formation in capillary breakup. *JFluid Mech*. 1992;243:297–317.
33. Cubaud T. Deformation and breakup of high-viscosity droplets with symmetric microfluidic cross flows. *Phys Rev E*. 2009;80:026307.
34. Basaran OA. Small-scale free surface flows with breakup: drop formation and emerging applications. *AIChE J*. 2002;48:1842–1848.
35. Eggers J. Nonlinear dynamics and breakup of free-surface flows. *Rev Mod Phys*. 1997;69:865–929.
36. Eggers J, Villermaux E. Physics of liquid jets. *Rep Prog Phys*. 2008;71:036601.
37. Leppinen D, Lister JR. Capillary pinch-off in inviscid fluids. *Phys Fluids*. 2003;15:568–578.
38. Wilkes ED, Phillips SD, Basaran OA. Computational and experimental analysis of dynamics of drop formation. *Phys Fluids*. 1999;11:3577–3598.
39. Funfschilling D, Debas H, Li HZ, Mason TG. Flow-field dynamics during droplet formation by dripping in hydrodynamic-focusing microfluidics. *Phys Rev E*. 2009;80:015301.
40. Lee W, Walker LM, Anna SL. Role of geometry and fluid properties in droplet and thread formation processes in planar flow focusing. *Phys Fluids*. 2009;21:032103.
41. Arratia PE, Thomas CC, Diorio J, Gollub JP. Elastic instabilities of polymer solutions in cross-channel flow. *Phys Rev Lett*. 2006;96:144502.
42. Cohen I, Nagel SR. Testing for scaling behavior dependence on geometrical and fluid parameters in the two fluid drop snap-off problem. *Phys Fluids*. 2001;13:3533–3541.
43. Castrejón-Pita JR, Castrejón-Pita AA, Thete SS, Sambath K, Hutchings LM, Hinch J, Lister JR, Basaran OA. Plethora of transitions during breakup of liquid filaments. *Proc Natl Acad Sci*. 2015;112:4582–4587.
44. Cooper-White JJ, Fagan JE, Tirtaatmadja V, Lester DR, Boger DV. Drop formation dynamics of constant low-viscosity, elastic fluids. *J NonNewtonian Fluid Mech*. 2002;106:29–59.
45. Wang X, Zhu C, Fu T, Ma Y. Bubble breakup with permanent obstruction in an asymmetric microfluidic T-Junction. *AIChE J*. 2015;61:1081–1091.
46. Fu T, Ma Y, Funfschilling D, Li HZ. Dynamics of bubble breakup in a microfluidic T-junction divergence. *Chem Eng Sci*. 2011;66:4184–4195.
47. Thoroddsen ST, Etoh TG, Takehara K. Experiments on bubble pinch-off. *Phys Fluids*. 2007;19:042101.

Manuscript received Jan. 27, 2015, and revision received June 12, 2015.